THERMAL BEHAVIOR, KINETICS AND SYNERGISTIC EFFECT OF CO-PYROLYSIS OF MOSO BAMBOO WITH BITUMINOUS COAL USING THERMOGRAVIMETRIC ANALYSIS AND ARTIFICIAL NEURAL NETWORK

Fengxia AN[1], Sheng WANG[1], Shaohua LIANG[2], Yu PENG[2], Miaomiao NIU[2]*

[1]State Key Laboratory of Low-Carbon Smart Coal-Fired Power Generation and Ultra-Clean Emission, China Energy Science and Technology Research Institute Co., Ltd., Nanjing, 210023, China

[*2]College of Energy and Power Engineering, Nanjing Institute of Technology, Nanjing, 211167, China

[*] Corresponding author; E-mail: niumiao8899@163.com

The thermal decomposition behavior, kinetics and interactions during co-pyrolysis of moso bamboo and bituminous coal were investigated by thermogravimetric analysis and artificial neural networks. Compared with bituminous coal, moso bamboo showed a lower initial pyrolysis temperature, a lower devolatilization stage and a higher decomposition rate. Co-pyrolysis involved devolatilization of moso bamboo at low temperature and devolatilization of bituminous coal at high temperature. With the blending of moso bamboo, the initial pyrolysis temperature showed a decrease of approximately 100 °C. The decomposition rate increased from 2.07 to 8.24 %/min, showing a larger devolatilization index and strengthened devolatilization reactivity. A higher heating rate accelerated the decomposition rate and strengthened char pyrolysis. As the heating rate increased, the devolatilization index could be doubled. The overall activation energy of co-pyrolysis was lower than that of individual coal pyrolysis, first decreasing and then increasing with moso bamboo blending. The minimum overall activation energy (~54 kJ/mol) for co-pyrolysis was found with a moso bamboo blending ratio of 25-40 %. Meanwhile, the activation energy proportion for moso bamboo devolatilization gradually increased with moso bamboo blending. Significant synergy was found with the moso bamboo blending ratio of 40-60 %, manifesting as a shift of the weight loss peak to higher temperature and an increase in the weight loss rate and degree. Trained artificial neural network models were built and optimized using the transfer function and hidden layers to predict the co-pyrolysis thermogravimetric profiles.

Key words*: co-pyrolysis; thermogravimetry analysis; kinetics; synergistic effect; artificial neural network*

1. Introduction

The thermochemical utilization of biomass could largely alleviate energy shortages and advance China's dual-carbon goal [1, 2]. However, biomass usually shows a relatively low energy density and has complex and various components, making the large-scale application challenging so far. The co-

processing of coal and biomass could not only enhance the clean utilization of coal but also dispose of biomass waste [3]. Pyrolysis is one of the most promising thermochemical conversion technology and also the initial stage of gasification and combustion. Investigation on the thermal behavior and synergistic effect during co-pyrolysis of biomass and coal could not only be beneficial to optimize the distribution and characteristics of pyrolysis product, but also get a full understanding of the subsequent gasification and combustion reactions. Zeng *et al.* [4] found that heating rate has a significant impact on the co-pyrolysis of long-flame coal and furfural residue. They observed that rapid infrared heating could upgrade co-pyrolysis oil quality, showing a positive synergistic effect for oil production. Pattanayak *et al.* [5] studied thermal performance and kinetic analysis during the co-pyrolysis of Indian bamboo and coal by thermogravimetric experiments, verifying the interactions between bamboo and coal. Laouge *et al.* [6] proved the synergistic effect during co-pyrolysis of pine sawdust and coal. They found that the pine sawdust blending ratio would directly influence the pyrolysis rate and the kinetic parameters (such as activation energy). However, due to the diversity of biomass and coal and the complexity of co-pyrolysis, current research on co-pyrolysis is still insufficient.

Many factors including temperature, blending ratio and heating rate could influence the behavior and interaction of co-pyrolysis [7]. But, considering the cost, time and material type, exploring all influencing factors by experiments is not practical. In this condition, artificial neural networks (ANNs) could offer a feasible research approach to co-pyrolysis by learning the relationships between the inputs and outputs of co-pyrolysis from the experimental data without a clear understanding of the mechanisms. ANN has been successfully applied to the analysis of various thermochemical processes [8], including lignite pyrolysis and combustion [9], oxygen-enriched combustion in gasoline engines [10], and biomass gasification [11]. Thus neural network technology could be used in the biomass-coal co-pyrolysis research.

Bamboo is an important forest resource in China and could be used as a sustainable resource owing to its excellent regeneration ability and high yield [12]. In this work, the co-pyrolysis of moso bamboo and bituminous coal was analyzed by thermogravimetric experiments and artificial neural networks. Thermogravimetric analysis of moso bamboo (Phyllostachys edulis), bituminous coal and their blends was conducted with different blending ratios and heating rates. The thermal decomposition behavior, kinetics and synergistic effect during co-pyrolysis were investigated. Based on the thermogravimetric experiment results, an artificial neural network model for co-pyrolysis was established, providing a comprehensive and in-depth analysis of the co-pyrolysis process. The work could help understanding biomass-coal co-pyrolysis characteristics and accelerate the co-pyrolysis applications at pilot scales.

2. Materials and Methods

2.1. Raw Materials

Moso bamboo from Jiangsu province and bituminous coal from Shaanxi province in China were selected as raw materials. Both samples were crushed to a particle size of no more than 0.3 mm and dried at 105 °C for 12 h to eliminate the influence of moisture. To prepare the blends, the two samples were first weighed and mixed according to the blending ratio and then crushed together to a particle size of no more than 0.3 mm for drying. The proximate analysis of moso bamboo and bituminous coal was performed according to the Chinese standards GB/T 28731-2012 and GB/T 212-2008, respectively. B0, B10, B25, B40, B50, B60, B75, B90 and B100 represent the biomass and coal mixture with biomass

blending ratios of 0 %, 10 %, 25 %, 40 %, 50 %, 60 %, 75 %, 90 % and 100 %, respectively. The properties of both fuels are shown in Tab. 1.

Table 1. Raw material properties

Material	Proximate analysis (%)				Ultimate analysis (%)					High heating value (MJ/kg)
	M_{ad}	A_{ad}	V_{daf}	FC_{daf}	C_{daf}	H_{daf}	N_{daf}	S_{daf}	O_{daf}	Q_{daf}
Moso bamboo	4.04	0.76	84.36	15.64	49.08	6.38	0.12	0.01	44.41	18.45
Bituminous coal	6.46	5.57	36.22	63.78	80.95	7.15	0.99	0.73	10.18	33.89

2.2. Thermogravimetric Analysis

Thermogravimetric analyses were conducted in a SDT650 thermogravimetric analyzer (TGA). For each test, the sample mass was kept at 6 ± 0.01 mg with a total nitrogen flow rate of 100 mL/min. The TGA temperature was increased from ambient temperature to 800 °C with heating rates of 10 °C/min, 20 °C/min and 30 °C/min. Thermogravimetric (TG) and differential thermogravimetric (DTG) curves were obtained for each sample.

As a non-isothermal model-fitting integral method, the Coats-Redfern integral method could be used for segmented analysis of the reaction mechanism and activity in different pyrolysis reaction stages [13]. Thus, it was suitable for the kinetic analysis of co-pyrolysis. The kinetic reactions were governed by Arrhenius law and could be described as follows:

$$\frac{d\alpha}{dt} = kf(\alpha) \tag{1}$$

$$k = Aexp(-\frac{E}{RT}) \tag{2}$$

$$\alpha = \frac{w_0 - w_t}{w_0 - w_f} \times 100\% \tag{3}$$

where α is the pyrolysis conversion of sample (on ash-free basis) at time *t*, %; *t* is the reaction time, min; $f(\alpha)$ refers to a selected model of the reaction mechanism, which has been shown in Tab. 2; *k* is the rate constant in the Arrhenius equation; *A* is the pre-exponential factor, min^{-1}; *E* is the activation energy, kJ/mol; *R* is the gas constant, 8.314 J/(mol·K); *T* is the absolute temperature, K; w_0 is the initial mass of the sample, mg; w_t is the mass of the sample at reaction time *t*, mg; w_f is the mass of the sample at the end of pyrolysis, mg.

During pyrolysis, a constant heating rate $\beta = dT/dt$, K/min was used. Substitute β into the above equations and the kinetics become:

$$\frac{d\alpha}{dT} = \frac{A}{\beta} exp(-\frac{E}{RT}) f(\alpha) \tag{4}$$

Equation (4) could be integrated and presented as below:

$$g(\alpha) = \int_0^\alpha d\alpha / f(\alpha) = \frac{A}{\beta} \int_{T_0}^{T} \exp(-E/RT)\, dT \tag{5}$$

where $g(\alpha)$ is the integral function of pyrolysis conversion; T_0 is the absolute temperature at the initial pyrolysis stage, K. Based on the Coats-Redfern method, Eq. (5) could be integrated and presented as below:

$$\ln\left(\frac{g(\alpha)}{T^2}\right) = \ln\left(\frac{AR}{\beta E}\left(1 - \frac{2RT}{E}\right)\right) - \frac{E}{RT} \tag{6}$$

Since the expression $\ln\left(\frac{AR}{\beta E}\left(1 - \frac{2RT}{E}\right)\right)$ is essentially constant, $\ln\left(\frac{g(\alpha)}{T^2}\right)$ has a linear relationship with 1/T. Thus linear equations in the form of y = ax + b could be obtained based on the linear fitting of

the thermogravimetric data according to Eq. (6). Here, "x" and "y" in the linear equations corresponded, respectively, to 1/T and $\ln\left(\frac{g(\alpha)}{T^2}\right)$. The fundamental function expressions of $f(\alpha)$ and $g(\alpha)$ could be determined by the reaction mechanism [14], as shown in Tab. 2. In order to estimate the values of E and A in this study, $g(\alpha)$ was first substituted using different expressions shown in Tab. 2 to determine the most suitable reaction mechanism model. Then the model was used for the calculation of E and A. Through the linear fitting of experimental data, the activation energy E and pre-exponential A could be calculated from the slope "a" and intercept "b" of the fitting line, respectively.

Table 2. Reaction mechanism models used in Coats and Redfern method

Reaction Model	Symbol	$f(\alpha)$	$g(\alpha)$	Mean R^2 (B50)	Mean F (B50)
First-order reaction	F1	$1-\alpha$	$-ln(1-\alpha)$	0.9850	809870
Second-order reaction	F2	$(1-\alpha)^2$	$(1-\alpha)^{-1}-1$	0.9750	221640
Avrami-Erofeev	A2	$2(1-\alpha)[-ln(1-\alpha)]^{1/2}$	$[-ln(1-\alpha)]^{1/2}$	0.9752	584418
Avrami-Erofeev	A3	$3(1-\alpha)[-ln(1-\alpha)]^{2/3}$	$[-ln(1-\alpha)]^{1/3}$	0.9484	369114

To verify the adequacy of the kinetic model, the F-Fisher's criteria was used [15] and could be calculated by the following equation:

$$F = \frac{\sum(\hat{y}_i-\bar{y})^2/1}{\sum(y_i-\hat{y}_i)^2/(n-2)} \quad (7)$$

where y_i is the experimental response to $(\ln\left(\frac{g(\alpha)}{T^2}\right))$; $\hat{y}_i$ is the fitted value; $\bar{y}$ is the mean of y_i; and n is the number of data points.

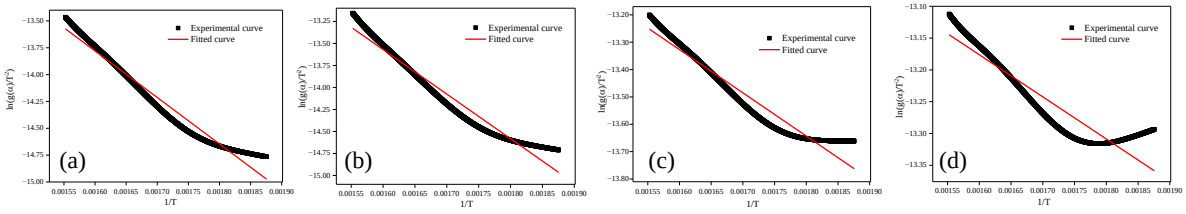

Figure 1. Linear fitting curve for B50 pyrolysis at 30°C/min; (a) F1 model, (b) F2 model, (c) A2 model, (d) A3 model

Kinetic models for B50 pyrolysis in the range 260-370 °C at heating rates of 10, 20 and 30 °C/min were built based on different mechanisms (F1, F2, A2 and A3). The mean values of regression coefficients (R^2) and F under three different heating rates during B50 pyrolysis for each model have been listed in Tab. 2. It could be found that the first-order reaction model showed the highest regression coefficients (R^2) and F value, indicating a good predication accuracy. Figure 1 shows the linear fitting curves for different models at 30 °C/min for B50 pyrolysis. The linear fitting of the F1 model also displayed the best fitting performance. Thus, in this research, the F1 model was used for the kinetic analysis of co-pyrolysis.

2.3. Co-Pyrolysis Characteristics

The devolatilization index (D_i) was applied to estimate pyrolysis performance. A higher value of D_i meant that the release of volatile was easier. The definition of D_i is as follows [16]:

$$D_i = \frac{(dw/dt)_{max}}{T_i T_{max} \Delta T_{1/2}} \quad (8)$$

where $(dw/dt)_{max}$ is the maximum decomposition rate, %/min; T_i is the initial pyrolysis temperature, °C; T_{max} is the temperature of maximum decomposition rate, °C; $\Delta T_{1/2}$ is the temperature interval when $dw/dt = 1/2(dw/dt)_{max}$, °C.

During co-pyrolysis, if there are differences between the actual experimental results and the theoretic results without synergy, the existence of interactions between the blended wastes could be proved. To analyze and evaluate the synergistic effect in the co-pyrolysis of biomass and coal, the experimental and calculated thermogravimetric results were compared. Theoretical results are calculated by Eq. (9), according to the proportionally weighted average of the results measured from individual pyrolysis.

$$w_{cal}(T) = \lambda_c w_c(T) + (1 - \lambda_c) w_b(T) \tag{9}$$

where w_{cal} is the weight-averaging calculated weight for blended fuel, mg; w_c is the experimental weight of bituminous coal, mg; w_b is the experimental weight of moso bamboo, mg; λ_c is the mass fraction of bituminous coal.

Taking the derivative of both sides of Eq. (9) with respect to reaction time, the theoretical weight loss rate dw/dt can be obtained as follows:

$$\frac{dw_{cal}(T)}{dt} = \lambda_c \frac{dw_c(T)}{dt} + (1 - \lambda_c) \frac{dw_b(T)}{dt} \tag{10}$$

By comparing the experimental results with the theoretical results without interaction, the interaction performance of the co-pyrolysis can be accurately evaluated.

2.4. Artificial Neural Network (ANN) Modeling

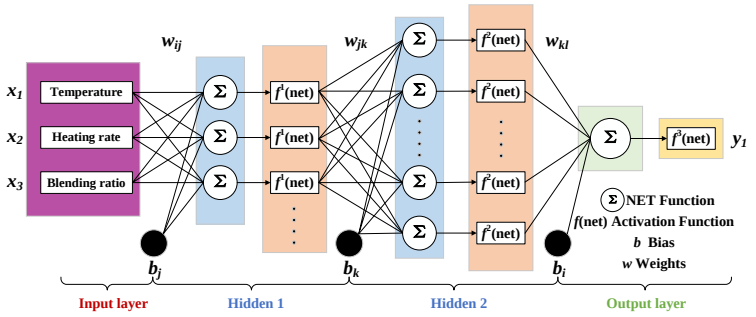

Figure 2. Structure diagram of ANN model

The Levenberg-Marquardt (LM) backpropagation algorithm with sigmoid function was used due to its fast convergence when solving non-linear numerical problems [17, 18]. As shown in Fig. 2, the ANN model consists of four major layers: input, hidden 1, hidden 2 and output. Pyrolysis temperature, blending ratio and heating rate were identified as model input parameters. The thermogravimetric data (mass loss) was considered as the output parameter. Connection between the adjacent layers could be achieved by one of the three distinct activation functions (tansig, logsig and purelin functions). The network performance of various activation function combinations based on ANN (3×5×1) was investigated with consistent iterations and learning rate. Comparing the mean absolute variance (MAE), mean square error (RMSE) and correlation coefficient (R^2) of different neural networks, the best artificial neural network can be obtained. Subsequently, based on the optimal activation function combination, an ANN model was constructed to study the influence of different neuron numbers. The model took 70 % of the data as the training set, 20 % as the validation set and 10 % as the test set. The

MAE, RMSE and R^2 can be calculated by Eq. (11)-(13). The smaller the error and the larger the R^2, the better trained the neural network and the more accurate the prediction.

$$MAE = \frac{1}{N}\left(\sum_{i=1}^{N}\left|H_i - H_{pi}\right|\right) \tag{11}$$

$$RMSE = \sqrt{\frac{1}{N}\left(\sum_{i=1}^{N}(H_i - H_{pi})^2\right)} \tag{12}$$

$$R^2 = 1 - \frac{\sum_{i=1}^{N}(H_i - H_{pi})^2}{\sum_{i=1}^{N}(H_i - \bar{H})^2} \tag{13}$$

where N is the number of iterations; H_i is the target value; H_{pi} is the output value of the model; $\bar{H}$ is the average target value.

3. Results and Discussion

3.1. Co-Pyrolysis Behavior

3.1.1 Effect of Blending Ratio

Figure 3 shows the thermogravimetric curve of co-pyrolysis of moso bamboo and bituminous coal with a heating rate of 10 °C/min. For individual pyrolysis, both materials underwent three stages with temperature: water evaporation, rapid devolatilization, and slow pyrolysis and reforming of char. The initial pyrolysis temperature of moso bamboo was significantly lower than that of bituminous coal, showing a relatively high weight loss rate during the rapid devolatilization stage. The main volatile releasing of moso bamboo was found within 200-400 °C while the volatile releasing of bituminous coal started above 400 °C. The devolatilization of the two materials occurred in distinct temperature ranges. This was mainly related to the different structure and connection methods of the organic components. Moso bamboo is mainly composed of cellulose, hemicellulose and lignin. Cellulose and hemicellulose start to decompose and release volatile matter above 160 °C [19]. Bituminous coal mainly consists of macromolecular organic structures. The depolymerization and cracking of active groups was mainly derived from the detachment of side chains in the macromolecular structure [20, 21], and the decomposition temperature of bituminous coal was higher. In the char pyrolysis stage, bituminous coal showed a small weight loss peak due to the high fixed carbon content, while bamboo showed no discernible peak. The total weight loss of bituminous coal and moso bamboo was less than 40 % and higher than 80 %, respectively.

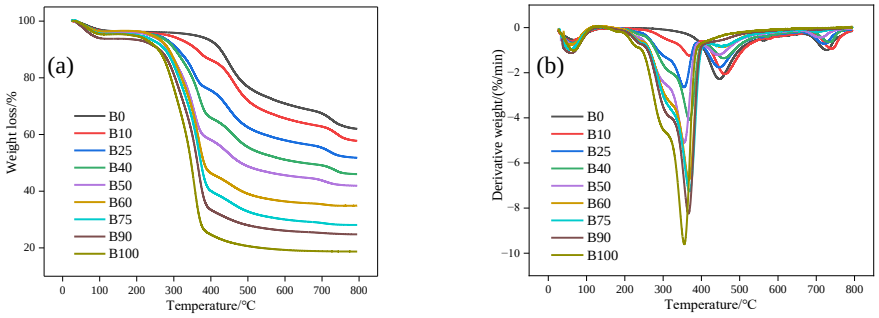

Figure 3. Thermogravimetric curve for co-pyrolysis with different blending ratios; (a) TG curve, (b) DTG curve

All the co-pyrolysis TG curves laid between the two individual pyrolysis TG curves, and the total weight loss gradually increased with bamboo blending. The devolatilization stage of co-pyrolysis

showed two independent weight loss peaks, corresponding to the devolatilization of moso bamboo and bituminous coal, respectively. Moso bamboo devolatilization peak was intensified and shifted to a lower temperature with moso bamboo blending, while the bituminous coal devolatilization peak gradually weakened. For 90 % moso bamboo blending, the weight loss peak of bituminous coal volatilization disappeared. Table 3 shows the co-pyrolysis parameters for different blending ratios with a heating rate of 10 °C/min. Compared with bituminous coal, the initial pyrolysis temperature of B10 dropped by approximately 100 °C. With moso bamboo addition, the initial pyrolysis temperature continuously dropped to approach the pyrolysis temperature of moso bamboo. The maximum decomposition rate of co-pyrolysis gradually increased and the temperature interval of the peak narrowed. The devolatilization index of co-pyrolysis continuously grew, indicating a higher volatile matter releasing activity of co-pyrolysis with biomass blending. Chen *et al.* [22] carried out co-pyrolysis of walnut sawdust and coal and also found the biomass blending could largely enhance the devolatilization index.

Table 3. Co-pyrolysis parameters with different blending ratios

Pyrolysis Parameter	B0	B10	B25	B40	B50	B60	B75	B90	B100
T_i (°C)	402.87	303.97	289.60	283.65	283.24	281.81	282.01	278.32	272.57
T_{max} (°C)	447.60	461.35	354.45	368.39	355.27	367.37	368.19	366.14	355.47
$(dw/dt)_{max}$ (%/min)	2.27	2.07	2.65	4.08	5.10	6.77	7.26	8.24	9.59
$\triangle T_{1/2}$ (°C)	80.03	80.03	61.36	58.69	61.36	58.69	64.02	53.35	56.02
D_i (10^{-7}%·min^{-1}·$°C^{-3}$)	1.57	1.84	4.21	6.65	8.26	11.14	10.92	15.16	17.67

3.1.2 Effect of Heating Rate

Figure 4 shows the DTG curves of B40, B50 and B60 blends with different heating rates. All DTG curves showed two distinct weight loss peaks in the devolatilization stage, corresponding to the volatile releasing of moso bamboo and bituminous coal, respectively. For a fixed blending ratio, the higher heating rate gradually shifted the two devolatilization weight loss peaks towards higher temperature, enhancing the co-pyrolysis decomposition rate in the whole range and intensifying the weight loss peaks. It is worth noting that a higher heating rate could effectively promote char pyrolysis. For the heating rate of 10 °C/min, the char pyrolysis weight loss peaks of the three co-pyrolysis conditions were not obvious. However, with a heating rate of 30 °C/min, B40, B50 and B60 pyrolysis all showed obvious weight loss peaks in the char pyrolysis stage.

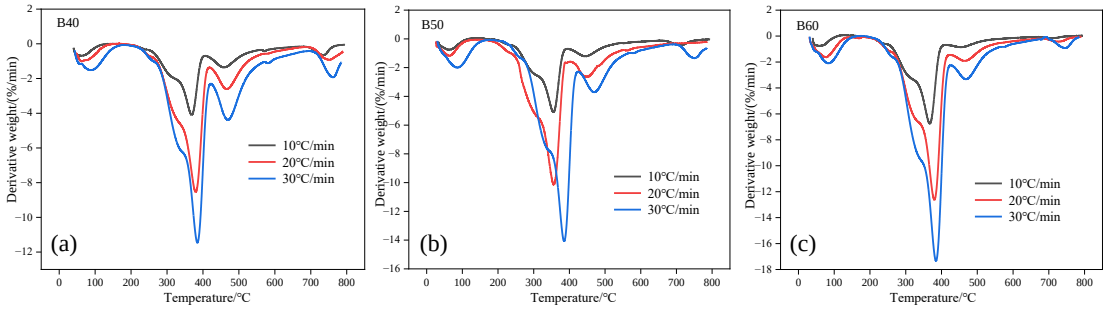

Figure 4. DTG curves for co-pyrolysis with different heating rates; (a) B40, (b) B50, (c) B60

Table 4 shows the co-pyrolysis parameters with different heating rates. The initial pyrolysis temperatures for all three blends increased with heating rate. This was mainly because the higher heating rate led to an increase in the temperature difference between the interior and surface of the sample,

delaying the co-pyrolysis to a certain extent [23]. This high-temperature delay raised the reaction temperature for the subsequent volatile matter releasing and char pyrolysis, further increasing the decomposition rate. The maximum decomposition rate was greatly improved with higher heating rate. From 10 °C/min to 20 °C/min, the maximum decomposition rate for all three blends doubled and the width of each weight loss peak was enlarged. All these changes resulted in a rapid increase in the devolatilization index, indicating a more active co-pyrolysis. Isah *et al.* [24] studied coal devolatilization during pyrolysis and found the coal macromolecules decomposed more quickly at higher heating rates.

Table 4. Co-pyrolysis parameters with different heating rates

Pyrolysis Parameter	B40	B40	B40	B50	B50	B50	B60	B60	B60
Heating rate (°C/min)	10	20	30	10	20	30	10	20	30
T_i (°C)	283.65	290.79	297.61	283.24	287.14	294.94	281.81	293.30	294.53
T_{max} (°C)	368.39	380.71	384.20	355.27	355.88	385.84	367.37	380.71	385.02
$(dw/dt)_{max}$ (%/min)	4.08	8.54	11.44	5.10	10.13	14.03	6.77	12.56	17.29
$\triangle T_{1/2}$ (°C)	58.69	69.35	74.69	61.36	74.70	74.70	58.69	72.02	74.69
D_i (10^{-7}%·min^{-1}·$°C^{-3}$)	6.65	11.12	13.40	8.26	13.27	16.50	11.14	15.62	20.41

3.2. Kinetic Analysis

Table 5 shows the kinetic parameters of co-pyrolysis based on the Coats-Redfern method. The regression coefficients (R^2) of the fitting lines were all higher than 0.97, indicating a good fitting match. Comparing the two individual pyrolysis, coal pyrolysis showed a relatively high active temperature range with a higher activation energy. Co-pyrolysis displayed two independent stages: the low-temperature range corresponded to the moso bamboo devolatilization and the high-temperature range corresponded to the bituminous coal devolatilization. For B10 pyrolysis, the activation energy of bituminous coal devolatilization was slightly higher and coal pyrolysis took a dominant role. For bamboo blending ratio higher than 25 %, moso bamboo devolatilization was gradually strengthened and became dominate. This was mainly related to the higher proportion of volatile matter, which would consume more heat for decomposition and require higher energy for bond breaking [25]. As a combined effect of heat-mass transfer and reaction interaction, raw materials with a higher proportion often exhibit a higher activation energy during co-pyrolysis [26, 27]. When the blending ratio of moso bamboo was higher than 60 %, the activation energy of bituminous coal dropped below 10 kJ/mol and its influence on co-pyrolysis was greatly reduced.

For the moso bamboo blending ratio within 10-50 %, the overall activation energy of co-pyrolysis was lower than that of individual coal pyrolysis. The overall activation energy first decreased and then increased with moso bamboo blending during co-pyrolysis. For the moso bamboo blending ratio of 90 %, co-pyrolysis only showed one active temperature range and the coal devolatilization was too weak for its activation energy to be calculated. The overall activation energy decreased and the co-pyrolysis was basically close to the moso bamboo pyrolysis.

Table 5. Kinetic analysis results of co-pyrolysis

Raw Material	Temperature (°C)	Activation Energy E (kJ/mol)	Overall Activation Energy E_a (kJ/mol)	Pre-Exponential Factor A (min^{-1})	Fitted Linear Equation	R^2
B0	390-530	60.29	60.29	3036.16	$y = -3.866 - 7251.169x$	0.9875

B10	300-400	24.79	58.50	4.45	y = −9.504 − 2981.816x	0.9881
	405-555	33.71		26.52	y = −8.025 − 4054.092x	0.9761
B25	260-370	34.67	54.37	74.61	y = −7.019 − 4169.837x	0.9880
	390-540	19.70		2.48	y = −9.859 − 2368.768x	0.9702
B40	260-372	40.77	54.88	307.00	y = −5.767 − 4903.617x	0.9906
	405-520	14.11		0.87	y = −10.568 − 1697.459x	0.9779
B50	260-370	48.18	59.46	2293.94	y = −3.922 − 5794.391x	0.9943
	400-520	11.28		0.56	y = −10.789 − 1357.031x	0.9797
B60	250-385	52.98	62.84	6248.39	y = −3.015 − 6371.794x	0.9883
	415-520	9.86		0.50	y = −10.762 − 1185.960x	0.9878
B75	250-385	47.85	55.14	2134.82	y = −3.987 − 5755.187x	0.9801
	410-520	7.29		0.25	y = −11.170 − 876.605x	0.9824
B90	245-380	46.47	46.47	1812.10	y = −4.122 − 5588.525x	0.9714
B100	240-372	52.87	52.87	9270.48	y = −2.619 − 6358.823x	0.9807

3.3. Interaction during Co-Pyrolysis

Figure 5 shows the comparison between the experimental and theoretical co-pyrolysis. With a moso bamboo blending ratio lower than 25 %, the theoretical TG and DTG curves were basically in line with the experimental curves. Interaction between the two materials was limited due to the small biomass addition. With increasing blending of moso bamboo, co-pyrolysis showed a more obvious interaction in the devolatilization stage. Compared with the theoretical DTG curve, the experimental weight loss peak shifted to a higher temperature and exhibited a higher maximum decomposition rate. For the moso bamboo blending ratio in the range of 40-60 %, the interaction in the devolatilization stage was most significant. As shown in Tab. 3, the initial temperature for moso bamboo pyrolysis (200-300 °C) was lower than that for bituminous coal (>350 °C). During the initial devolatilization stage, the presence of bituminous coal particles would result in diffusion resistance and heat transfer shielding for the moso bamboo devolatilization, inhibiting and delaying the moso bamboo pyrolysis [28]. However, the delay in moso bamboo devolatilization could also increase the reaction temperature, enhancing the activity of volatile matter release and improving the decomposition rate. When the moso bamboo blending ratio increased to 60 %, compared to the theoretical results, the experimental weight loss was significantly higher and the residual char yield was greatly decreased.

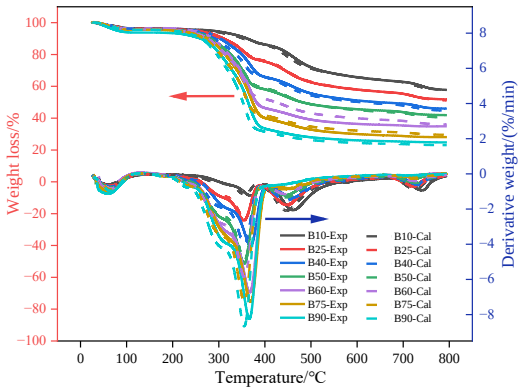

Figure 5. Comparison between the experimental and theoretical results (Exp: experimental results, Cal: calculated results)

Due to the devolatilization shift towards a high temperature, a high-temperature shift in the weight loss peak occurred in the char pyrolysis stage with a small change in the char decomposition rate. In addition, co-processing hindered the heat transfer in the coal particles and led to a delay in the char pyrolysis [29]. Above 75 % moso bamboo, char-pyrolysis interaction faded: the DTG peak shifted less and actual weight loss nearly matched the calculated value. According to the kinetic analysis, for moso bamboo blending ratios above 75 %, the co-pyrolysis was dominated by moso bamboo pyrolysis and the interaction during char pyrolysis weakened. Overall, when the blending ratio of bituminous coal and moso bamboo was basically equal, co-pyrolysis showed a more obvious interaction, shifting DTG curve towards high temperature and intensifying pyrolysis conversion. When the blending ratio of a certain raw material was relatively high, the interaction during the co-pyrolysis process became small. The result was consistent with the research of Guo *et al.* [27], who found that the co-pyrolysis synergistic effect gradually diminished as biomass proportion increased.

3.4. Artificial Neural Network Prediction

Table 6 shows the network performance of different activation function combinations based on ANN (3×5×1). For the LTP (logsig-tansig-purelin) activation function combination, the neural network showed the smallest MAE value (1.0157) and RMSE value (1.5039), as well as the largest R^2 value (0.9968). Therefore, the optimal combination of activation functions for the neural network in this work was LTP.

Table 6. Network performance of different activation function combinations

Input	Activation Function Combination	Network Topology	MAE	RMSE	R^2
Temperature	TTT	3×5×1	1.2324	1.7057	0.9959
Blending ratio	TTL		8.1914	14.443	0.7085
Heating rate	TTP		1.1958	1.6986	0.9960
	TLT		1.4091	1.9092	0.9949
	TLL		8.0566	14.4344	0.7089
	TLP		1.3094	1.7992	0.9955
	TPT		2.5373	3.0489	0.9869
	TPL		8.7193	14.5390	0.7023
	TPP		2.3512	3.2287	0.9853
	LTT		1.1253	1.5353	0.9967
	LTL		8.1899	14.4432	0.7085
	LTP		1.0157	1.5039	0.9968
	LLT		1.2120	1.7160	0.9959
	LLL		8.1902	14.4409	0.7086
	LLP		1.1851	1.6736	0.9961
	LPT		2.4614	2.9975	0.9873
	LPL		8.6153	14.5015	0.7038
	LPP		2.3512	3.2287	0.9853
	PTT		1.4122	1.8794	0.9951
	PTL		8.4725	14.4898	0.7060

PTP	1.5737	2.0599	0.9941
PLT	1.4854	2.0514	0.9941
PLL	8.4392	14.4836	0.7063
PLP	1.6025	2.1458	0.9936
PPT	7.1328	9.2430	0.8798
PPL	10.6355	15.1845	0.6755
PPP	8.9847	10.9063	0.8333

T: tansig function; L: logsig function; P: purelin function.

Based on the optimal activation function combination (LTP), 25 ANN models were constructed with different neuron numbers in each hidden layer. Table 7 shows the MAE, RMSE and R^2 of the 25 models. The total number of iteration steps in the models was 10,000, while the performance goal was 10^{-4}. The main training results indicated that the ANN-24 model exhibited the optimal performance, showing the smallest MAE (0.3411) and RMSE (0.4854) and the largest R^2 (0.9997). Thus, the ANN-24 could be considered as the optimal model for predicting the co-pyrolysis of moso bamboo and bituminous coal. Fig. 6 shows the network topology for the optimal ANN model, where the number of neurons in hidden layers 1 and 2 were 7 and 15, respectively. Fig. 7 shows the regression coefficients of the ANN-24 model.

Table 7. Comparison of the performance parameters of 25 ANN models

Model	Input	Output	Network Topology	MAE	RMSE	R^2
ANN-1	Temperature	TG	3×1×1	1.6185	2.1413	0.9935
ANN-2	Blending ratio		3×3×1	1.3560	1.7865	0.9955
ANN-3	Heating rate		3×5×1	1.0157	1.5039	0.9968
ANN-4			3×7×1	1.1715	1.5109	0.9968
ANN-5			3×9×1	0.9713	1.3344	0.9975
ANN-6			3×11×1	1.8958	3.3636	0.9843
ANN-7			3×13×1	0.9900	1.4182	0.9972
ANN-8			3×15×1	0.7749	1.1371	0.9982
ANN-9			3×17×1	1.0248	1.5214	0.9968
ANN-10			5×3×1	1.1361	1.5637	0.9966
ANN-11			5×5×1	1.0681	1.4707	0.9970
ANN-12			5×7×1	0.7719	1.0713	0.9984
ANN-13			5×9×1	0.8037	1.1199	0.9983
ANN-14			5×11×1	0.6485	0.9424	0.9988
ANN-15			5×13×1	0.5537	0.8202	0.9991
ANN-16			5×15×1	0.4627	0.6881	0.9993
ANN-17			5×17×1	0.6935	1.0668	0.9984
ANN-18			7×3×1	1.0500	1.4328	0.9971
ANN-19			7×5×1	0.6786	0.9639	0.9987
ANN-20			7×7×1	0.5798	0.9236	0.9988
ANN-21			7×9×1	0.6111	1.0523	0.9985
ANN-22			7×11×1	0.7057	1.0682	0.9984
ANN-23			7×13×1	0.5332	0.7799	0.9992
ANN-24			7×15×1	0.3411	0.4854	0.9997

ANN-25	7×17×1	0.4257	0.7842	0.9991

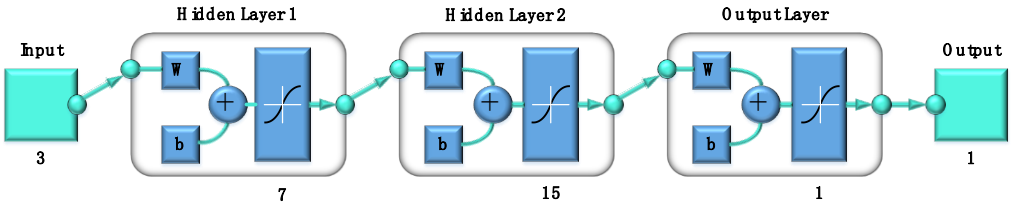

Figure 6. Network topology of ANN-24 model

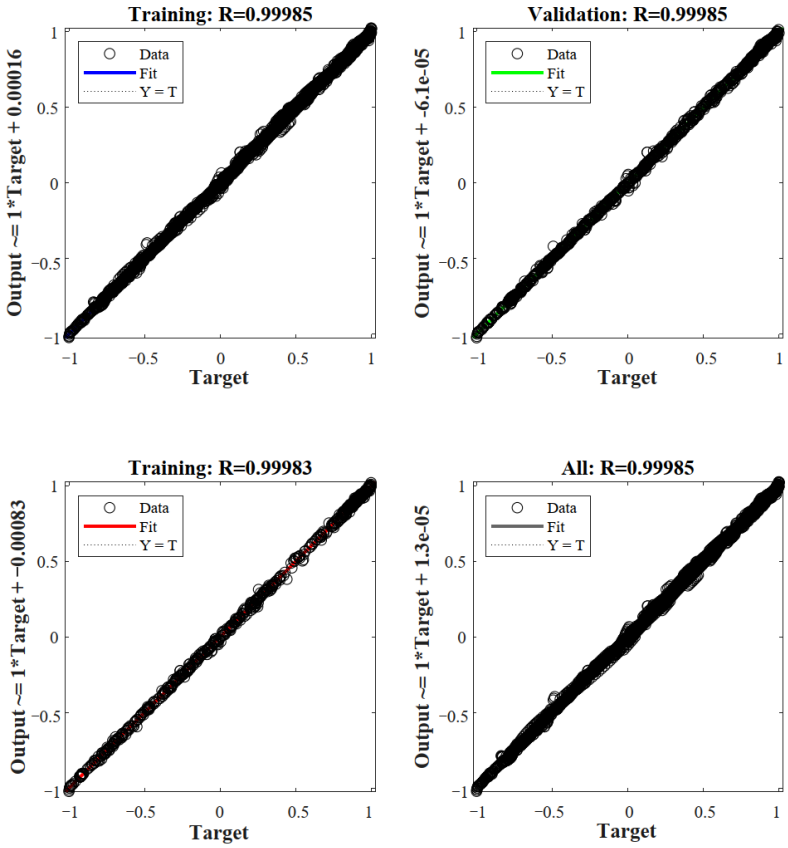

Figure 7. Regression coefficients of ANN-24 model

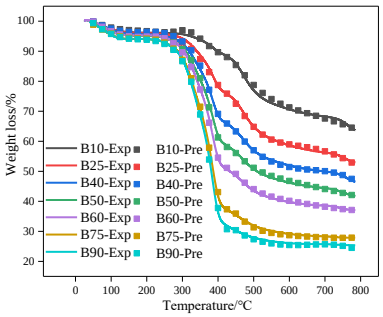

Figure 8. ANN predicted and experimental TG results at 30°C/min (Exp: experimental results, Pre: ANN-24 predicted results)

Figure 8 shows the comparison of the predicted TG value based on the ANN-24 model and experimental TG value. The predicted TG results were almost identical to the experimental TG value, indicating good accuracy of the ANN-24 model.

4. Conclusions

In this work, the thermal behavior, kinetics and synergistic effect during co-pyrolysis of moso bamboo and bituminous coal were studied by thermogravimetric experiments. An artificial neural network model was built to accurately predict the co-pyrolysis characteristics. Effects of the moso bamboo blending ratio and heating rate on co-pyrolysis performance were analyzed. Compared with bituminous coal, moso bamboo showed a lower initial pyrolysis temperature, a lower devolatilization stage and a higher decomposition rate. Co-pyrolysis displayed independent moso bamboo and bituminous coal devolatilization stages. Moso bamboo blending declined the initial pyrolysis temperature by about 100 °C, intensified devolatilization and improved the devolatilization index. A higher heating rate greatly enhanced the co-pyrolysis reaction rate and strengthened char pyrolysis. With the heating rate increased from 10 to 30 °C/min, the devolatilization index could be doubled. The minimum overall activation energy (~54 kJ/mol) was found for the moso bamboo blending ratio of 25-40%. Moso bamboo blending enhanced the activation energy of moso bamboo devolatilization, making moso bamboo pyrolysis gradually dominant. Obvious interaction was observed with comparable biomass and coal contents, shifting the weight loss peak to a high temperature and improving the decomposition rate. ANN-24, with 7 neurons in hidden layer 1 and 15 neurons in hidden layer 2, was selected as the optimal model for co-pyrolysis prediction.

Acknowledgment

The authors acknowledge the financial support from the National Natural Science Foundation of China (51906100, 12305186), the Natural Science Foundation of Jiangsu Province (BK20191015), Jiangsu Province 333 High-level Talent Project, the Innovation Foundation of Nanjing Institute of Technology (CKJA202302) and the Open Foundation of State Key Laboratory of Low-Carbon Smart Coal-Fired Power Generation (D2022FK094).

References

[1] Adeleke, A. A., *et al.*, A comprehensive review on the similarity and disparity of torrefied biomass and coal properties, *Renewable and Sustainable Energy Reviews*, *199* (2024), pp. 114502

[2] Wei, W., *et al.*, Dual carbon goals and the impact on future agricultural development in China: a general equilibrium analysis, *China Agricultural Economic Review*, *14* (2022), 4, pp. 664-685

[3] Niu, M., *et al.*, Synergistic effect on combustion kinetics and ash fusion characteristics during co-combustion of bituminous coal and wheat straw, *Thermal Science*, *29* (2025), 5 Part A, pp. 3615-3628

[4] Zeng, Y. F., *et al.*, Insight into impact of co-pyrolysis process parameters on cross-interaction of volatiles between furfural residue and coal via rapid infrared heating, *Energy*, *309* (2024), pp. 133118

[5] Pattanayak, S., *et al.*, Thermal performance and synergetic behaviour of co-pyrolysis of North East Indian bamboo biomass with coal using thermogravimetric analysis, *Biomass Conversion and Biorefinery*, *13* (2023), 13, pp. 11755-11768

[6] Laougé, Z. B., Merdun, H., Investigation of thermal behavior of pine sawdust and coal during co-pyrolysis and co-combustion, *Energy*, *231* (2021), pp. 120895

[7] Niu, M., *et al.*, Synergistic effect on thermal behavior and product characteristics during co-pyrolysis of biomass and waste tire: Influence of biomass species and waste blending ratios, *Energy*, *240* (2022), pp. 122808
[8] Yang, H., *et al.*, An ANN-based method for predicting Zhundong and other Chinese coal slagging potential, *Fuel*, *293* (2021), pp. 120271
[9] Prabhakaran, S. P. S., *et al.*, Combustion and pyrolysis kinetics of Australian lignite coal and validation by artificial neural networks, *Energy*, *242* (2022), pp. 122949
[10] Sun, P., *et al.*, Prediction of oxygen-enriched combustion and emission performance on a spark ignition engine using artificial neural networks, *Applied Energy*, *348* (2023), pp. 121466
[11] Ascher, S., *et al.*, A comprehensive artificial neural network model for gasification process prediction, *Applied Energy*, *320* (2022), pp. 119289
[12] Zhang, H., *et al.*, Charting the Research Status for Bamboo Resources and Bamboo as a Sustainable Plastic Alternative: A Bibliometric Review, *Forests*, *15* (2024), 10, pp. 1812
[13] Huang, X.-J., *et al.*, Pyrolysis kinetic analysis of sequential extract residues from Hefeng subbituminous coal based on the Coats-Redfern method, *ACS omega*, *7* (2022), 25, pp. 21397-21406
[14] Merdun, H., *et al.*, Synergistic effects on co-pyrolysis and co-combustion of sludge and coal investigated by thermogravimetric analysis, *Journal of Thermal Analysis Calorimetry*, *146* (2021), 6, pp. 2623-2637
[15] Pyshyev, S., *et al.*, Creation of experimental-statistical and kinetic models of the coumarone-indene-carbazole resin production process, *Results in Engineering*, *25* (2025), pp. 103689
[16] Wu, Z., *et al.*, Thermal Behavior and Char Structure Evolution of Bituminous Coal Blends with Edible Fungi Residue during Co-Pyrolysis, *Energy & Fuels*, *28* (2014), 3, pp. 1792-1801
[17] Kanthasamy, R., *et al.*, Bayesian optimized multilayer perceptron neural network modelling of biochar and syngas production from pyrolysis of biomass-derived wastes, *Fuel*, *350* (2023), pp. 128832
[18] Mohammadi, M.-R., *et al.*, Application of cascade forward neural network and group method of data handling to modeling crude oil pyrolysis during thermal enhanced oil recovery, *Journal of Petroleum Science and Engineering*, *205* (2021), pp. 108836
[19] Wang, S., *et al.*, Lignocellulosic biomass pyrolysis mechanism: A state-of-the-art review, *Progress in Energy and Combustion Science*, *62* (2017), pp. 33-86
[20] Liu, C., *et al.*, Molecular structure model construction and pyrolysis mechanism study on low-rank coal by experiments and ReaxFF simulations, *Journal of Analytical and Applied Pyrolysis*, *178* (2024), pp. 106387
[21] Niu, M., *et al.*, Insight into the Formation and Evolution Mechanism of Char and Volatiles During Biomass Pyrolysis: Thermal Behavior Analysis and Free Radical Investigation, *Combust. Sci. Technol.* (2025), pp. 1-21
[22] Chen, X., *et al.*, Pyrolysis Characteristics and Kinetics of Coal–Biomass Blends during Co-Pyrolysis, *Energy & Fuels*, *33* (2019), 2, pp. 1267-1278
[23] Cao, R., *et al.*, Research on the pyrolysis characteristics and mechanisms of waste printed circuit boards at fast and slow heating rates, *Waste Management*, *149* (2022), pp. 134-145
[24] Isah, U. A., *et al.*, Kinetics and heating rates effects on coal devolatilization during pyrolysis, *Thermochim. Acta*, *748* (2025), pp. 179999
[25] Liu, N., *et al.*, Co-Pyrolysis behavior of coal and biomass: synergistic effect and kinetic analysis, *ACS omega*, *9* (2024), 29, pp. 31803-31813
[26] Bhattacharyya, M., *et al.*, Co-pyrolysis of coal and biomass blends: Impact of pyrolysis temperature and biomass blending on thermal stability of coal, and composition of pyrolysis products, *Process Safety and Environmental Protection*, *187* (2024), pp. 1010-1021
[27] Guo, Z., *et al.*, Co-pyrolysis and co-combustion characteristics of low-rank coal and waste biomass: Insights into interactions, kinetics and synergistic effects, *Journal of the Energy Institute*, *118* (2025), pp. 101918
[28] Chen, X., *et al.*, Pyrolysis characteristics and kinetics of coal–biomass blends during co-pyrolysis, *Energy & fuels*, *33* (2019), 2, pp. 1267-1278
[29] Li, S., *et al.*, Co-pyrolysis characteristic of biomass and bituminous coal, *Bioresource Technology*, *179* (2015), pp. 414-420

Submitted: 30.11.2025.
Revised: 14.01.2026
Accepted: 19.01.2026.